

# Spin-State Dependence of Exchange-Correlation Holes

Julia Brüggemann, Christoph R. Jacob<sup>1</sup>

Technische Universität Braunschweig, Institute of Physical and Theoretical Chemistry,  
Gaußstraße 17, 38106 Braunschweig, Germany

Date: June 10, 2020

---

<sup>1</sup>E-Mail: [c.jacob@tu-braunschweig.de](mailto:c.jacob@tu-braunschweig.de)

## Table of Contents Graphics

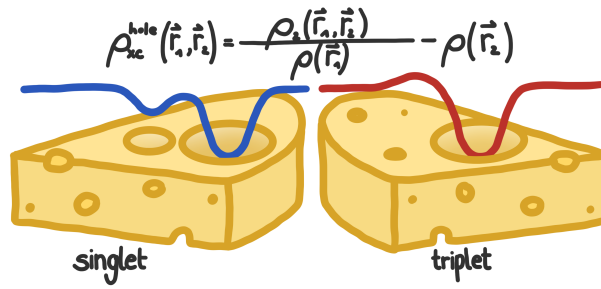


## Table of Contents Text

The exchange–correlation holes of different spin states are analyzed, as a step towards explicitly spin-state dependent density-functional approximations.

## Abstract

Applications of density functional theory (DFT) in computational chemistry rely on an approximate exchange-correlation (xc) functional. However, existing approximations can fail dramatically for open-shell molecules, in particular for transition-metal complexes or radicals. Most importantly, predicting energy-differences between different spin-states with approximate exchange-correlation functionals remains extremely challenging. Formally, it is known that the exact xc functional should be spin-state dependent, but none of the available approximations features such an explicit spin-state dependence [Ch. R. Jacob, M. Reiher, *Int. J. Quantum Chem.*, 2012, **112**, 3661–3684]. Thus, to find novel approximations for the xc functional for open-shell systems, the development of spin-state dependent xc functionals appears to be a promising avenue. Here, we set out to shed light on the spin-state dependence of the xc functional by investigating the underlying xc holes, which we extract from configuration interaction calculations for model systems. We analyze the similarities and differences between the xc holes of the lowest-energy singlet and triplet states of the dihydrogen molecule, the helium atom, and the lithium dimer. To shed further light on the spin-state dependence of these xc holes we also discuss exact conditions that can be derived from the spin structure of the reduced two-electron density matrix. Altogether, our results suggest several possible routes towards the construction of explicitly spin-state dependent approximations for the xc functional.

# 1 Introduction

Density-functional theory (DFT) is widely applied for studying functional open-shell molecules. Computational studies of, e.g., electronic and magnetic properties of transition metal centers,<sup>1–5</sup> transition-metal catalyzed reaction mechanisms,<sup>6–9</sup> spectroscopic properties of open-shell reaction centers,<sup>10–14</sup> or spin-dependent electron transport,<sup>15,16</sup> mostly rely on the availability of approximate exchange–correlation (xc) functionals that are applicable for open-shell molecules.

However, despite intense research in the past decades, such density-functional approximations (DFAs) are still plagued by a “spin-state problem”, i.e., a lack of predictive power for energy differences between different spin states. Generally, such spin-state energy differences are highly dependent on the chosen approximate xc functional.<sup>2,17–19</sup> In a pioneering work, Reiher *et al.* found an approximately linear dependence on the exact exchange admixture and proposed a hybrid functional tuned for spin-state energetics in iron complexes.<sup>20</sup> Subsequently, several generalized-gradient approximation and hybrid xc functional with a good performance for specific classes of systems have been identified,<sup>21,22</sup> and novel approximate functional have been developed for spin-state energetics.<sup>23,24</sup> Nevertheless, the choice of an approximate xc functional that performs satisfactorily for spin-state energetics generally requires careful benchmarking.

On the other hand, wave-function based quantum-chemical calculations rarely offer a feasible alternative to the use of DFAs. In most cases, the prediction of spin-state energy differences requires a multireference treatment in combination with a balanced inclusion of dynamical correlation<sup>25–27</sup> as provided by CASPT2 and related multireference methods.<sup>8,28,29</sup> However, these show an exponential scaling of the computational effort with respect to the size of the active space. While approaches based on the density-matrix renormalization group (DMRG) algorithm<sup>30–32</sup> applied to the calculation of spin-state

energies<sup>33,34</sup> can significantly reduce this scaling, approaches for the balanced inclusion of dynamical correlation in DMRG are still under development.<sup>35–37</sup> Emerging methods combining a multireference treatment with DFT might also be promising for spin-state energetics,<sup>38–41</sup> but all such methods still rely on the definition of an active space and thus scale unfavorably with system size.

To gain insights into possible novel approaches for addressing the spin-state problem of DFAs, one of us has previously reviewed the exact theory underlying DFT for open-shell systems.<sup>42</sup> Formally, the Hohenberg–Kohn (HK) theorems<sup>43</sup> make no reference to spin. When defining the universal HK functional via the Levy constrained search formalism<sup>44,45</sup> as,

$$F_{\text{HK}}[\rho] = \min_{\Psi \rightarrow \rho} \langle \Psi | \hat{T} + \hat{V}_{\text{ee}} | \Psi \rangle, \quad (1)$$

where the constrained search includes all normalized, antisymmetric wavefunctions  $\Psi$  that yield the electron density  $\rho(\mathbf{r})$ , one notices that neither knowledge of the spin density nor of the spin state of the system are required. Instead, the variational principle provided by the second HK theorem<sup>43</sup> will lead to the ground state, irrespective of its spin symmetry.

However, such a formulation is generally not useful, but instead one commonly targets the lowest-energy state of a given spin symmetry (i.e., corresponding to a chosen eigenvalue of  $\hat{\mathbf{S}}^2$ ). This implies the definition of a spin-state specific HK functional,<sup>46</sup>

$$F_{\text{HK}}^S[\rho] = \min_{\Psi^S \rightarrow \rho} \langle \Psi^S | \hat{T} + \hat{V}_{\text{ee}} | \Psi^S \rangle \quad \text{with} \quad \hat{\mathbf{S}}^2 \Psi^S = S(S+1) \Psi^S, \quad (2)$$

where the constrained search now includes only those normalized, antisymmetric wavefunctions  $\Psi^S$  that are eigenfunctions of  $\hat{\mathbf{S}}^2$  with eigenvalue  $S(S+1)$ . Being able to target the lowest-energy state for each spin symmetry is a prerequisite for the calculation of the energy differences between spin states with DFT.

The above definition of a spin-state specific HK functional translates to the definition of an explicitly spin-state specific xc functional  $E_{\text{xc}}^S[\rho]$ . However, none of the currently available

DFAs feature such an explicit spin-state dependence. Instead, the spin-state dependence is included implicitly by formulating DFAs in terms of not only the total electron density  $\rho(\mathbf{r})$ , but also the spin density  $Q(\mathbf{r}) = \rho_\alpha(\mathbf{r}) - \rho_\beta(\mathbf{r})$ , and by simultaneously restricting the treatment to the multiplet state with maximal eigenvalue of  $\hat{S}_z$  (i.e., with  $M_S = S$ ). This, in turn, mandates a violation of the fractional spin condition<sup>47–49</sup> that must hold for the exact spin-density dependent functional. Thus, DFAs that obey this exact constraint must feature an explicit spin-state dependence that is modeled independently of the spin-density dependence. For an in-depth discussion, we refer to Ref. 42.

As a first step towards the development of explicitly spin-state dependent approximations to the xc functional, in this work we investigate the spin-state dependence of the xc hole,<sup>50–52</sup>

$$\rho_{\text{xc}}^{\text{hole}}(\mathbf{r}_2|\mathbf{r}_1) = \frac{\rho_2(\mathbf{r}_1, \mathbf{r}_2)}{\rho(\mathbf{r}_1)} - \rho(\mathbf{r}_2), \quad (3)$$

where  $\rho_2(\mathbf{r}_1, \mathbf{r}_2)$  is the electron pair density. The xc hole describes the change in the probability of finding a second electron at position  $\mathbf{r}_2$ , given that there is a first electron at position  $\mathbf{r}_1$ . The study of properties of xc holes has provided valuable insights<sup>52,53</sup> that have guided the development of approximate xc functionals.<sup>54</sup> Many modern approximate xc functionals are based on explicit models of the xc hole.<sup>55–59</sup>

This work is organized as follows. In Sect. 2 we review the necessary theoretical background and discuss analytical properties of the spin-state dependent xc hole. In Sect. 3 we revisit the seminal work of Baerends and coworkers on the xc hole in the H<sub>2</sub> molecule<sup>52,53</sup> and compare different ways of visualizing xc holes. In Sect. 4 we then present xc holes extracted from accurate wavefunction-based calculations for two-electron systems, specifically for the H<sub>2</sub> molecule and the helium atom in their lowest-energy singlet and triplet states, and turn to the lowest-energy singlet and triplet states of the lithium dimer as a simple many-electron test case in Sect. 5. Finally, our conclusions as well as possible routes towards the construction of explicitly spin-state dependent exchange–correlation

functionals are discussed in Sect. 6. The Computational Details are given at the end of this paper.

## 2 Theoretical Background: Spin in DFT

### 2.1 Spin-States in DFT

For a molecule in the absence of an external magnetic field with the non-relativistic electronic Hamiltonian (in atomic units),

$$\hat{H} = \hat{T} + \hat{V}_{\text{nuc}} + \hat{V}_{\text{ee}} \quad (4)$$

where  $\hat{T}$  is the kinetic-energy operator,  $\hat{V}_{\text{nuc}}$  is the operator of the electron–nuclear attraction, and  $\hat{V}_{\text{ee}}$  is the operator of the electron–electron repulsion, the eigenfunctions of  $\hat{H}$  can always be chosen as simultaneous eigenfunctions of the operator of the squared total spin  $\hat{S}^2$  (with eigenvalue  $S(S+1)$ ,  $S = 0, \frac{1}{2}, 1, \dots$ ) and of the operator of the  $z$ -component of the total spin  $M_S$  (with eigenvalue  $M_S = -S, \dots, +S$ ). While states with different  $S$ , commonly termed *spin states*, generally have different energies, for one spin state the  $2S + 1$  eigenfunctions with different  $M_S$  (multiplet states) are always degenerate.

DFT relies on the HK theorem, which states that the ground-state energy  $E_0$  and electron density  $\rho(\mathbf{r})$  can be determined by minimizing the total energy functional,

$$E[\rho] = F_{\text{HK}}[\rho] + \int v_{\text{nuc}}(\mathbf{r})\rho(\mathbf{r}) \, d^3r, \quad (5)$$

with the universal HK functional defined in Eq. (1) and the nuclear potential  $v_{\text{nuc}}(\mathbf{r})$ . Following Gunnarson and Lundquist,<sup>46</sup> this procedure can be extended to the lowest-energy state with a specific  $S$  by using the spin-state specific total energy functional,

$$E^S[\rho] = F_{\text{HK}}^S[\rho] + \int v_{\text{nuc}}(\mathbf{r})\rho(\mathbf{r}) \, d^3r, \quad (6)$$

with the spin-state specific HK functional defined in Eq. (2). As is discussed in Ref. 42, the definitions of the HK functional and of the total energy functional can be extended to include a dependence on the spin density  $Q(\mathbf{r}) = \rho_\alpha(\mathbf{r}) - \rho_\beta(\mathbf{r})$ . While this is necessary for accessing the spin density of the lowest-energy states in addition to their total electron density, this spin-density dependence is formally independent from the spin-state dependence. This is also dictated by the fractional spin condition for the exact HK functional.<sup>47–49</sup> As an inclusion of the spin-density dependence raises numerous additional intricacies,<sup>42</sup> we will only consider spin-density independent functionals in this work.

In the Kohn–Sham (KS) formalism of DFT, the spin-state dependent universal HK functional is decomposed as,

$$\begin{aligned}
F_{\text{HK}}^S[\rho] &= T^S[\rho] + V_{\text{ee}}^S[\rho] \\
&= T_s[\rho] + J[\rho] + V_{\text{ee,xc}}^S[\rho] + T_c^S[\rho] \\
&= T_s[\rho] + J[\rho] + E_{\text{xc}}^S[\rho].
\end{aligned} \tag{7}$$

In the first line, the general kinetic and electron–electron repulsion energy functionals  $T^S[\rho]$  and  $V_{\text{ee}}^S[\rho]$  can be defined via the Levy constrained search formalism.<sup>44,45</sup> The kinetic energy functional is further decomposed into the noninteracting kinetic energy  $T_s[\rho]$ , which is defined via the KS reference system of noninteracting electrons, and a correlation contribution  $T_c^S[\rho] = T^S[\rho] - T_s[\rho]$ . Similarly, the electron–electron repulsion energy is decomposed into the classical Coulomb energy is given by

$$J[\rho] = \frac{1}{2} \iint \frac{\rho(\mathbf{r}_1)\rho(\mathbf{r}_2)}{|\mathbf{r}_1 - \mathbf{r}_2|} d^3r_1 d^3r_2 \tag{8}$$

and a nonclassical (exchange–correlation) contribution  $V_{\text{ee,xc}}^S[\rho] = V_{\text{ee}}^S[\rho] - J[\rho]$ . Finally, the exchange–correlation (xc) energy functional is defined as the sum of the two non-classical contributions,

$$E_{\text{xc}}^S[\rho] = V_{\text{ee,xc}}^S[\rho] + T_c^S[\rho] = V_{\text{ee,xc}}^S[\rho] - J[\rho] + T_c^S[\rho]. \tag{9}$$

As the Coulomb energy depends only on the electron density, it is obviously spin-state independent. Within a spin-density independent KS formalism, it is shown in Ref. 42 that different spin-states of the non-interacting reference system are always degenerate with a state with  $S = 0$  (for an even number of electrons) or  $S = \frac{1}{2}$  (for an odd number of electrons). Therefore,  $T_s[\rho]$  becomes spin-state independent. Thus, the spin-state dependence of the HK functional is fully contained in the spin-state dependence of the xc functional.

## 2.2 Spin-Structure of the Reduced Density Matrices

Before further analyzing the spin-state dependence of the xc functional, it is instructive to revisit the spin-structure of the reduced density matrices<sup>60,61</sup> that provide the link between the spin state and the electron–electron interaction. The Levy constrained search in Eq. (1) or Eq. (2) defines an implicit mapping from the electron density  $\rho(\mathbf{r})$  to the many-electron wavefunction  $\Psi(\mathbf{x}_1, \mathbf{x}_2, \dots, \mathbf{x}_N)$ , where  $\mathbf{x}_i = (\mathbf{r}_i, s_i)$  combines spatial and spin coordinates of the  $i$ th electron. From this wavefunction, one can obtain the two-electron reduced density matrix (2-RDM),

$$\Gamma_2(\mathbf{x}_1, \mathbf{x}_2, \mathbf{x}'_1, \mathbf{x}'_2) = N(N-1) \int \dots \int \Psi(\mathbf{x}_1, \mathbf{x}_2, \mathbf{x}_3, \dots, \mathbf{x}_N) \times \Psi^*(\mathbf{x}_1, \mathbf{x}_2, \mathbf{x}_3, \dots, \mathbf{x}_N) d\mathbf{x}_3 \dots d\mathbf{x}_N \quad (10)$$

as well as the one-electron reduced density matrix (1-RDM),

$$\Gamma_1(\mathbf{x}_1, \mathbf{x}'_1) = \frac{1}{N-1} \int \Gamma_2(\mathbf{x}_1, \mathbf{x}_2, \mathbf{x}'_1, \mathbf{x}_2) d\mathbf{x}_2 \quad (11)$$

from which the (spin-resolved) electron density can be obtained as  $\rho(\mathbf{x}) = \Gamma_1(\mathbf{x}, \mathbf{x})$ .

The density matrices defined above can be decomposed into different spin components.

The 2-RDM formally consists of sixteen spin components,

$$\begin{aligned}
\Gamma_2(\mathbf{x}_1, \mathbf{x}_2, \mathbf{x}'_1, \mathbf{x}'_2) &= \Gamma_2^{\alpha\alpha\alpha\alpha}(\mathbf{r}_1, \mathbf{r}_2, \mathbf{r}'_1, \mathbf{r}'_2) \alpha(s_1)\alpha(s_2)\alpha(s'_1)\alpha(s'_2) \\
&+ \Gamma_2^{\alpha\alpha\alpha\beta}(\mathbf{r}_1, \mathbf{r}_2, \mathbf{r}'_1, \mathbf{r}'_2) \alpha(s_1)\alpha(s_2)\alpha(s'_1)\beta(s'_2) \\
&+ \Gamma_2^{\alpha\alpha\beta\alpha}(\mathbf{r}_1, \mathbf{r}_2, \mathbf{r}'_1, \mathbf{r}'_2) \alpha(s_1)\alpha(s_2)\beta(s'_1)\beta(s'_2) \\
&+ \cdots + \Gamma_2^{\beta\beta\beta\beta}(\mathbf{r}_1, \mathbf{r}_2, \mathbf{r}'_1, \mathbf{r}'_2) \beta(s_1)\beta(s_2)\beta(s'_1)\beta(s'_2). \tag{12}
\end{aligned}$$

However, for eigenstates of  $\hat{S}_z$  only six of these components, namely  $\Gamma_2^{\alpha\alpha\alpha\alpha}$ ,  $\Gamma_2^{\beta\beta\beta\beta}$ ,  $\Gamma_2^{\alpha\beta\alpha\beta}$ ,  $\Gamma_2^{\beta\alpha\beta\alpha}$ ,  $\Gamma_2^{\alpha\beta\beta\alpha}$ , and  $\Gamma_2^{\beta\alpha\alpha\beta}$  are nonzero.<sup>61</sup> Since the 2-RDM is formed from an antisymmetric wavefunction,  $\Gamma_2$  has to be antisymmetric with respect to the exchange of  $\mathbf{x}_1 \leftrightarrow \mathbf{x}_2$  and of  $\mathbf{x}'_1 \leftrightarrow \mathbf{x}'_2$ . It follows that  $\rho_2^{\alpha\alpha\alpha\alpha}$  and  $\rho_2^{\beta\beta\beta\beta}$  are antisymmetric themselves, and that the other four nonzero components are related by

$$\begin{aligned}
\Gamma_2^{\alpha\beta\alpha\beta}(\mathbf{r}_1, \mathbf{r}_2, \mathbf{r}'_1, \mathbf{r}'_2) &= -\Gamma_2^{\alpha\beta\beta\alpha}(\mathbf{r}_2, \mathbf{r}_1, \mathbf{r}'_1, \mathbf{r}'_2) \\
&= -\Gamma_2^{\alpha\beta\beta\alpha}(\mathbf{r}_1, \mathbf{r}_2, \mathbf{r}'_2, \mathbf{r}'_1) = \Gamma_2^{\beta\alpha\beta\alpha}(\mathbf{r}_2, \mathbf{r}_1, \mathbf{r}'_2, \mathbf{r}'_1). \tag{13}
\end{aligned}$$

Therefore, only three independent components of the two-electron density matrix  $\rho_2$  remain.<sup>60,61</sup> McWeeny and Mizuno<sup>60</sup> introduced the following three independent components, which are particularly convenient for an analysis of the spin structure of the 2-RDM,

$$\begin{aligned}
A(\mathbf{r}_1, \mathbf{r}_2, \mathbf{r}'_1, \mathbf{r}'_2) &= \Gamma_2^{\alpha\alpha\alpha\alpha}(\mathbf{r}_1, \mathbf{r}_2, \mathbf{r}'_1, \mathbf{r}'_2) + \Gamma_2^{\alpha\beta\alpha\beta}(\mathbf{r}_1, \mathbf{r}_2, \mathbf{r}'_1, \mathbf{r}'_2) \\
&+ \Gamma_2^{\beta\alpha\beta\alpha}(\mathbf{r}_1, \mathbf{r}_2, \mathbf{r}'_1, \mathbf{r}'_2) + \Gamma_2^{\beta\beta\beta\beta}(\mathbf{r}_1, \mathbf{r}_2, \mathbf{r}'_1, \mathbf{r}'_2) \tag{14}
\end{aligned}$$

$$\begin{aligned}
B(\mathbf{r}_1, \mathbf{r}_2, \mathbf{r}'_1, \mathbf{r}'_2) &= \Gamma_2^{\alpha\alpha\alpha\alpha}(\mathbf{r}_1, \mathbf{r}_2, \mathbf{r}'_1, \mathbf{r}'_2) + \Gamma_2^{\alpha\beta\alpha\beta}(\mathbf{r}_1, \mathbf{r}_2, \mathbf{r}'_1, \mathbf{r}'_2) \\
&- \Gamma_2^{\beta\alpha\beta\alpha}(\mathbf{r}_1, \mathbf{r}_2, \mathbf{r}'_1, \mathbf{r}'_2) - \Gamma_2^{\beta\beta\beta\beta}(\mathbf{r}_1, \mathbf{r}_2, \mathbf{r}'_1, \mathbf{r}'_2) \tag{15}
\end{aligned}$$

$$\begin{aligned}
C(\mathbf{r}_1, \mathbf{r}_2, \mathbf{r}'_1, \mathbf{r}'_2) &= \Gamma_2^{\alpha\alpha\alpha\alpha}(\mathbf{r}_1, \mathbf{r}_2, \mathbf{r}'_1, \mathbf{r}'_2) - \Gamma_2^{\alpha\beta\alpha\beta}(\mathbf{r}_1, \mathbf{r}_2, \mathbf{r}'_1, \mathbf{r}'_2) - \Gamma_2^{\beta\alpha\beta\alpha}(\mathbf{r}_1, \mathbf{r}_2, \mathbf{r}'_1, \mathbf{r}'_2) \\
&- \Gamma_2^{\alpha\beta\beta\alpha}(\mathbf{r}_1, \mathbf{r}_2, \mathbf{r}'_1, \mathbf{r}'_2) - \Gamma_2^{\beta\alpha\alpha\beta}(\mathbf{r}_1, \mathbf{r}_2, \mathbf{r}'_1, \mathbf{r}'_2) + \Gamma_2^{\beta\beta\beta\beta}(\mathbf{r}_1, \mathbf{r}_2, \mathbf{r}'_1, \mathbf{r}'_2) \tag{16}
\end{aligned}$$

It can be shown<sup>60</sup> that for a given spin state  $S$ , the 2-RDM components of the multiplet

states with different  $M_S$  are related by

$$A^{M_S}(\mathbf{r}_1, \mathbf{r}_2, \mathbf{r}'_1, \mathbf{r}'_2) = A^{M_S=S}(\mathbf{r}_1, \mathbf{r}_2, \mathbf{r}'_1, \mathbf{r}'_2) \quad (17)$$

$$B^{M_S}(\mathbf{r}_1, \mathbf{r}_2, \mathbf{r}'_1, \mathbf{r}'_2) = \begin{cases} 0 & \text{for } S = 0 \\ \left(\frac{M_S}{S}\right) B^{M_S=S}(\mathbf{r}_1, \mathbf{r}_2, \mathbf{r}'_1, \mathbf{r}'_2) & \text{for } S \leq \frac{1}{2} \end{cases} \quad (18)$$

$$C^{M_S}(\mathbf{r}_1, \mathbf{r}_2, \mathbf{r}'_1, \mathbf{r}'_2) = \begin{cases} 0 & \text{for } S = 0, \frac{1}{2} \\ \left(\frac{3M_S^2 - S(S+1)}{S(2S-1)}\right) C^{M_S=S}(\mathbf{r}_1, \mathbf{r}_2, \mathbf{r}'_1, \mathbf{r}'_2) & \text{for } S \leq 1 \end{cases} \quad (19)$$

While  $A(\mathbf{r}_1, \mathbf{r}_2, \mathbf{r}'_1, \mathbf{r}'_2)$  is the same for all multiplet states, their  $B(\mathbf{r}_1, \mathbf{r}_2, \mathbf{r}'_1, \mathbf{r}'_2)$  and  $C(\mathbf{r}_1, \mathbf{r}_2, \mathbf{r}'_1, \mathbf{r}'_2)$  are related by a simple linear scaling. As the different multiplet states are degenerate, one can always choose the state with  $M_S = 0$  (or an equivalent ensemble<sup>42</sup>) in the Levy constrained search in Eq. (1) or Eq. (2), which implies  $B(\mathbf{r}_1, \mathbf{r}_2, \mathbf{r}'_1, \mathbf{r}'_2) = C(\mathbf{r}_1, \mathbf{r}_2, \mathbf{r}'_1, \mathbf{r}'_2) = 0$ . Of course,  $A(\mathbf{r}_1, \mathbf{r}_2, \mathbf{r}'_1, \mathbf{r}'_2)$ ,  $B(\mathbf{r}_1, \mathbf{r}_2, \mathbf{r}'_1, \mathbf{r}'_2)$ , and  $C(\mathbf{r}_1, \mathbf{r}_2, \mathbf{r}'_1, \mathbf{r}'_2)$  are implicitly linked by the fact that they emerge from the same antisymmetric wavefunction  $\Psi(\mathbf{x}_1, \dots, \mathbf{x}_N)$ , which in turn implicitly depends on the electron density.

The expectation value of the electron–electron interaction is determined by the electron pair density  $\rho_2(\mathbf{r}_1, \mathbf{r}_2)$ , which is given by the diagonal of  $A(\mathbf{r}_1, \mathbf{r}_2, \mathbf{r}'_1, \mathbf{r}'_2)$ ,

$$\langle \Psi | \hat{V}_{ee} | \Psi \rangle = \frac{1}{2} \iint \frac{\rho_2(\mathbf{r}_1, \mathbf{r}_2)}{|\mathbf{r}_1 - \mathbf{r}_2|} d^3r_1 d^3r_2 = \frac{1}{2} \iint \frac{A(\mathbf{r}_1, \mathbf{r}_2, \mathbf{r}_1, \mathbf{r}_2)}{|\mathbf{r}_1 - \mathbf{r}_2|} d^3r_1 d^3r_2. \quad (20)$$

Here, the electron pair density  $\rho_2(\mathbf{r}_1, \mathbf{r}_2)$  is the probability density for finding a first electron at position  $\mathbf{r}_1$  and a second electron at position  $\mathbf{r}_2$ . For later use, we also introduce the on-top pair density  $\rho_2(\mathbf{r}, \mathbf{r})$ , which is the probability density for simultaneously finding two electrons at position  $\mathbf{r}$ .

The expectation value of the total spin operator is also determined by  $A(\mathbf{r}_1, \mathbf{r}_2, \mathbf{r}'_1, \mathbf{r}'_2)$ ,<sup>60</sup>

$$\langle \Psi | \hat{\mathbf{S}}^2 | \Psi \rangle = -\frac{1}{4} \iint \left( A(\mathbf{r}_1, \mathbf{r}_2, \mathbf{r}_1, \mathbf{r}_2) + 2A(\mathbf{r}_2, \mathbf{r}_1, \mathbf{r}_1, \mathbf{r}_2) \right) d^3r_1 d^3r_2 + \frac{3}{4}N. \quad (21)$$

Thus, the system's electron–electron repulsion and its spin state are linked via  $A(\mathbf{r}_1, \mathbf{r}_2, \mathbf{r}'_1, \mathbf{r}'_2)$ , and changing the spin state will affect the electron–electron interaction energy. The difficulty of capturing this implicit link in the construction of approximate xc functionals is at the root of the spin-state problem of current DFAs.

The spin structure of the 1-RDM now directly follows from the spin structure of the 2-RDM and Eq. (11). For eigenstates of  $\hat{S}_z$ , there are only two independent spin components,  $\Gamma_1^{\alpha\alpha}(\mathbf{r}_1, \mathbf{r}'_1)$  and  $\Gamma_1^{\beta\beta}(\mathbf{r}_1, \mathbf{r}'_1)$  or alternatively, a total density matrix

$$\rho_1(\mathbf{r}_1, \mathbf{r}'_1) = \frac{1}{N-1} \int A(\mathbf{r}_1, \mathbf{r}_2, \mathbf{r}'_1, \mathbf{r}_2) d^3r_2 = \Gamma_1^{\alpha\alpha}(\mathbf{r}_1, \mathbf{r}'_1) + \Gamma_1^{\beta\beta}(\mathbf{r}_1, \mathbf{r}'_1) \quad (22)$$

and a spin density matrix,

$$Q_1(\mathbf{r}_1, \mathbf{r}'_1) = \frac{1}{N-1} \int B(\mathbf{r}_1, \mathbf{r}_2, \mathbf{r}'_1, \mathbf{r}_2) d^3r_2 = \Gamma_1^{\alpha\alpha}(\mathbf{r}_1, \mathbf{r}'_1) - \Gamma_1^{\beta\beta}(\mathbf{r}_1, \mathbf{r}'_1), \quad (23)$$

from which the total electron density  $\rho(\mathbf{r}) = \rho_1(\mathbf{r}, \mathbf{r}) = \rho_\alpha(\mathbf{r}) + \rho_\beta(\mathbf{r})$  and the spin density  $Q(\mathbf{r}) = Q_1(\mathbf{r}, \mathbf{r}) = \rho_\alpha(\mathbf{r}) - \rho_\beta(\mathbf{r})$  emerge as their diagonals.

The relation between the spin density matrices (and the spin densities) of the degenerate multiplet states,<sup>42, 60</sup>

$$Q_1^{M_S}(\mathbf{r}_1, \mathbf{r}'_1) = \begin{cases} 0 & \text{for } S = 0 \\ \left(\frac{M_S}{S}\right) Q_1^{M_S=0}(\mathbf{r}_1, \mathbf{r}'_1) & \text{for } S \leq \frac{1}{2} \end{cases} \quad (24)$$

is a direct consequence of Eq. (18), and translates to the fractional spin condition<sup>47–49</sup> discussed earlier.

### 2.3 The Exchange–Correlation Hole

For independent, uncorrelated electrons the pair density would be given by the product of the electron densities for the two electrons,

$$\rho_2^{\text{uncorr}}(\mathbf{r}_1, \mathbf{r}_2) = \rho(\mathbf{r}_1)\rho(\mathbf{r}_2). \quad (25)$$

The true pair density for correlated electrons can then be expressed as the sum of this uncorrelated pair density and a correction term,

$$\rho_2(\mathbf{r}_1, \mathbf{r}_2) = \rho(\mathbf{r}_1)\rho(\mathbf{r}_2) + \rho_2^{\text{xc}}(\mathbf{r}_1, \mathbf{r}_2), \quad (26)$$

where the correction term  $\rho_2^{\text{xc}}(\mathbf{r}_1, \mathbf{r}_2)$  accounts for exchange and correlation. The expectation value of the electron–electron repulsion energy [cf. Eq. (20)] then becomes

$$\begin{aligned} \langle \Psi | \hat{V}_{\text{ee}} | \Psi \rangle &= \frac{1}{2} \iint \frac{\rho(\mathbf{r}_1)\rho(\mathbf{r}_2)}{|\mathbf{r}_1 - \mathbf{r}_2|} d^3r_1 d^3r_2 + \frac{1}{2} \iint \frac{\rho_2^{\text{xc}}(\mathbf{r}_1, \mathbf{r}_2)}{|\mathbf{r}_1 - \mathbf{r}_2|} d^3r_1 d^3r_2 \\ &= J[\rho] + V_{\text{ee,xc}}^S[\rho], \end{aligned} \quad (27)$$

where the functionals of the Coulomb interaction and of the non-classical part of the electron–electron interaction have already been introduced above in Eq. (7).

This can be recast in a different form by starting from the conditional probability of finding a second electron at position  $\mathbf{r}_2$ , given that the first electron is at position  $\mathbf{r}_1$ ,

$$P^{\text{cond}}(\mathbf{r}_2|\mathbf{r}_1) = \frac{\rho_2(\mathbf{r}_1, \mathbf{r}_2)}{\rho(\mathbf{r}_1)} = \rho(\mathbf{r}_2) + \rho_{\text{xc}}^{\text{hole}}(\mathbf{r}_2|\mathbf{r}_1) \quad (28)$$

with the exchange–correlation hole,

$$\rho_{\text{xc}}^{\text{hole}}(\mathbf{r}_2|\mathbf{r}_1) = \frac{\rho_2^{\text{xc}}(\mathbf{r}_1, \mathbf{r}_2)}{\rho(\mathbf{r}_1)} = \frac{\rho_2(\mathbf{r}_1, \mathbf{r}_2)}{\rho(\mathbf{r}_1)} - \rho(\mathbf{r}_2). \quad (29)$$

The non-classical part of the electron–electron interaction then becomes

$$V_{\text{ee,xc}}^S[\rho] = \frac{1}{2} \iint \frac{\rho_{\text{xc}}^{\text{hole}}(\mathbf{r}_2|\mathbf{r}_1)}{|\mathbf{r}_1 - \mathbf{r}_2|} d^3r_2 \rho(\mathbf{r}_1) d^3r_1 \quad (30)$$

and the exchange–correlation energy functional can be expressed as

$$E_{\text{xc}}^S[\rho] = \frac{1}{2} \iint \frac{\rho_{\text{xc}}^{\text{hole}}(\mathbf{r}_2|\mathbf{r}_1)}{|\mathbf{r}_1 - \mathbf{r}_2|} d^3r_2 \rho(\mathbf{r}_1) d^3r_1 + T_c^S[\rho]. \quad (31)$$

In these expressions, the spin-state dependence of the functionals emerges via the implicit dependence of the wavefunction, and thus also of the exchange–correlation hole, on the electron density via the Levy constrained search of Eq. (2).

To elegantly handle the correlation contribution to the kinetic energy,  $T_c^S[\rho]$ , one can invoke the adiabatic connection between the noninteracting (coupling constant  $\lambda = 0$  and the fully interacting system ( $\lambda = 1$ ), while keeping the electron density constant. It can be shown<sup>51</sup> that the xc energy functional is then given by

$$E_{\text{xc}}[\rho] = \frac{1}{2} \iint \frac{\bar{\rho}_{\text{xc}}^{\text{hole}}(\mathbf{r}_2|\mathbf{r}_1)}{|\mathbf{r}_1 - \mathbf{r}_2|} d^3r_2 \rho(\mathbf{r}_1) d^3r_1, \quad (32)$$

with the coupling constant averaged xc hole,

$$\bar{\rho}_{\text{xc}}^{\text{hole}}(\mathbf{r}_2|\mathbf{r}_1) = \int_0^1 \lambda \rho_{\text{xc}}^{\text{hole}}(\mathbf{r}_2|\mathbf{r}_1) d\lambda, \quad (33)$$

where  $\lambda \rho_{\text{xc}}^{\text{hole}}(\mathbf{r}_2|\mathbf{r}_1)$  denotes the xc hole at coupling strength  $\lambda$ . In the present work, we will only consider the bare xc hole  $\rho_{\text{xc}}^{\text{hole}}(\mathbf{r}_2|\mathbf{r}_1)$ , but we note that an extension to coupling-strength averaged xc holes is possible using the technology introduced by Teale and coworkers.<sup>62–64</sup>

### 3 Visualization of XC Holes

Studying the xc holes extracted from accurate wavefunction-based calculations can provide valuable insights<sup>52</sup> and guide the development of approximate xc functionals. In fact, most approximate xc functionals currently in use are based on a model of the coupling-constant averaged xc hole.<sup>54</sup> As the xc hole depends on the spatial coordinates of both the position of the reference electron  $\mathbf{r}_1$  and of the second electron  $\mathbf{r}_2$ , its visualization will require some simplification of this six-dimensional quantity. First, we fix the position of the reference electron at  $\mathbf{r}_1 = \mathbf{r}_{\text{ref}}$ . For visualizing the remaining three spatial dimensions  $\mathbf{r}_2 = \mathbf{r}$ , different representations are possible, some of which will be discussed in the following. Each reveals different features of the xc hole, and a combination of these different representations will thus be required for our subsequent analysis of the spin-state dependence of the xc hole.

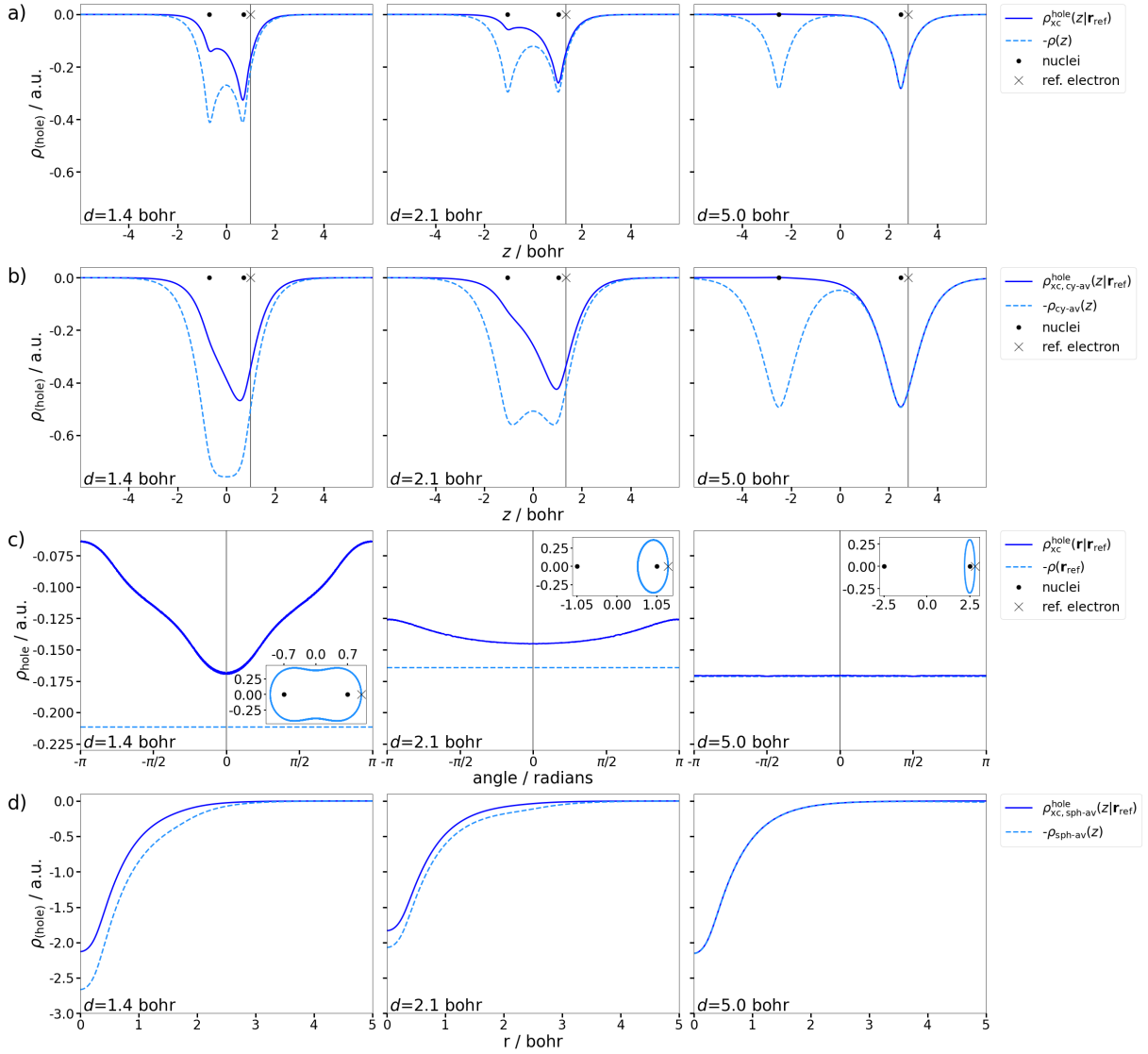


Figure 1: Negative electron density  $-\rho(\mathbf{r})$  (solid blue line) and exchange–correlation hole  $\rho_{xc}^{\text{hole}}(\mathbf{r}|\mathbf{r}_{\text{ref}})$  (dashed light blue line) in the singlet ground state of the H<sub>2</sub> molecule for an internuclear distance  $d$  of 1.4 bohr (left), 2.1 bohr (middle), and 5.0 bohr (right). All data has been obtained from Full-CI calculations using the cc-pVTZ basis set, and the reference electron has been placed on the internuclear  $z$ -axis at a distance of 0.3 bohr from the right hydrogen atom (indicated by a cross in the plots). (a) Plot of  $-\rho(z)$  and  $\rho_{xc}^{\text{hole}}(z|\mathbf{r}_{\text{ref}})$  along the internuclear  $z$ -axis. (b) Plot of the cylindrically-averaged negative density  $-\rho_{\text{cy-av}}(z)$  and xc hole  $\rho_{xc,\text{cy-av}}^{\text{hole}}(z|\mathbf{r}_{\text{ref}})$  [cf. Eq. (35)]. (c) Plot of  $\rho_{xc}^{\text{hole}}(\mathbf{r}|\mathbf{r}_{\text{ref}})$  on a contour of constant electron density through the position of the reference electron (see inset for a visualization of these isodensity contours in the  $xz$ -plane); (d) Plot of the spherically-averaged negative density  $-\rho_{\text{sph-av}}(r)$  and xc hole  $\rho_{xc,\text{sph-av}}^{\text{hole}}(r|\mathbf{r}_{\text{ref}})$  [cf. Eq. (36)].

Plots of the negative electron density and of the xc hole for the singlet ground state of the  $\text{H}_2$  molecule at different bond distances, which have been extracted from full configuration interaction (Full-CI) calculations (see Section “Computational Details”), are presented in Fig. 1. Here, we place the reference electron at position  $\mathbf{r}_1 = \mathbf{r}_{\text{ref}}$  at a distance of 0.3 bohr from the right hydrogen atom. In Fig. 1a, the negative density and xc hole are shown along the internuclear  $z$ -axis. These are in agreement with those obtained in the seminal work of Baerends and coworkers.<sup>52,53</sup>

The xc hole in the singlet ground state of the  $\text{H}_2$  molecule can be decomposed into the contributions of an exchange and a correlation hole.<sup>52</sup> For a closed-shell two electron system, the exchange hole, which cancels the self-interaction that is contained in the uncorrelated pair density, is equal to  $-\frac{1}{2}\rho(\mathbf{r})$ , i.e., it is delocalized over the whole molecule. The correlation hole is negative in the vicinity of the reference electron, while it is positive further away from the reference electron. For the equilibrium structure of  $\text{H}_2$  ( $d = 1.4$  bohr), this results in an xc hole that is mostly localized at the hydrogen atom close to the reference electron, but that also extends to the other hydrogen atom. When increasing the bond distance, the depth of the correlation hole at the hydrogen atom close to the reference electron increases, while simultaneously its positive contribution at the other hydrogen atom increases (left–right correlation). For the dissociated  $\text{H}_2$  molecule, the correlation hole fully cancels the exchange hole at the other hydrogen atom and the xc hole thus becomes fully localized at the hydrogen atom close to the reference electron.

While the decomposition into an exchange and a correlation hole can be useful for an initial discussion, an important finding of the work of Baerends and coworkers<sup>52</sup> was the fact that the xc hole is always more localized than the individual exchange and correlation holes. In many cases, this should simplify the construction of approximations for the xc hole. In fact, most available approximate xc functionals rely at least partly on an error cancelation between the exchange and correlation parts. For this reason, we will only

discuss the properties of the total xc hole in the following.

The normalization of the xc hole is given by,

$$\int \rho_{\text{xc}}^{\text{hole}}(\mathbf{r}|\mathbf{r}_{\text{ref}}) d^3r = -1. \quad (34)$$

However, this normalization cannot be inferred in the plots along the  $z$ -axis shown in Fig. 1a. Instead, the area under the curve changes with increasing bond distance. To recover the normalization of the xc hole in the visualization, Fig. 1b plots the cylindrically-averaged density and xc hole, i.e.,

$$\rho_{\text{xc, cy-av}}^{\text{hole}}(z|\mathbf{r}_{\text{ref}}) = \int_0^{2\pi} \int_0^\infty \rho_{\text{xc}}^{\text{hole}}(\mathbf{r} = r, \varphi, z|\mathbf{r}_{\text{ref}}) r dr d\varphi \quad (35)$$

where  $r, \varphi, z$  are defined in a cylindrical coordinate system, and where the cylindrically-averaged density is defined analogously. Note that because of the symmetry of the  $\text{H}_2$  molecule and the placement of the reference electron on the internuclear  $z$ -axis, the density and xc hole are independent of  $\varphi$ .

The features of the xc hole that were discussed above can also be recognized in the cylindrically-averaged plots shown in Fig. 1b, but the large peaks at the nuclei are now smoothed because of the averaging. For the density, the area under the curve now corresponds to the number of electrons, while for the xc hole it corresponds to its normalization. Note that, in contrast to the plots along the  $z$ -axis in Fig. 1a, the depth on the xc hole [i.e.,  $\rho_{\text{xc}}^{\text{hole}}(\mathbf{r}_{\text{ref}}|\mathbf{r}_{\text{ref}})$ ] cannot be extracted from the cylindrically-averaged plots.

In the plots considered so far, the short-range behavior of the xc hole in the vicinity of the reference electron is masked by the second term in Eq. (29), i.e., by the change of the electron density itself. To uncover this short-range behavior more clearly, Fig. 1c plots the xc hole on isodensity contours that correspond to the electron density at the position of the reference electron (shown as insets). The contour is followed by using the angle  $\varphi$  in polar coordinates with respect to the midpoint between the two nuclei or around the

nucleus close to the reference electron. In both cases,  $\varphi = 0$  corresponds to the position of the reference electron.

As the second term in Eq. (29) is constant on the isodensity contours and the denominator in the first term is the fixed density at the position of the reference electron, the plots in Fig. 1c reflect the change of the electron pair density  $\rho_2(\mathbf{r}, \mathbf{r}_{\text{ref}})$ . For the  $\text{H}_2$  molecule at its equilibrium bond distance, the xc hole along the isodensity contour is smallest at the position of the reference electron. The Coulomb repulsion of the reference electron reduces the probability of finding a second electron in its vicinity (“Coulomb hole”). Note that for the exact wavefunction, the plots would show a cusp at the position of the reference electron, which is only partly recovered by our finite-basis set calculations.<sup>65</sup> When increasing the bond distance, the plots of the xc hole become flatter, and in the dissociation limit, the xc hole is constant along the isodensity contour. This reflects the earlier observation that the xc hole becomes fully localized at the nucleus close to the reference electron and the probability of finding a second electron at the same nucleus becomes zero.

Finally, Fig. 1d shows plots of the spherically-averaged negative density and xc hole,

$$\rho_{\text{xc, sph-av}}^{\text{hole}}(r|\mathbf{r}_{\text{ref}}) = \int_0^{2\pi} \int_0^\pi \rho_{\text{xc}}^{\text{hole}}(\mathbf{r} = r, \theta, \varphi|\mathbf{r}_{\text{ref}}) \sin\theta d\theta d\varphi \quad (36)$$

where  $r, \theta, \varphi$  are defined in a spherical coordinate system, and where the spherically-averaged density is defined analogously. Here, the normalization of the xc hole is recovered by integrating  $r^2 \rho_{\text{xc, sph-av}}^{\text{hole}}(r|\mathbf{r}_{\text{ref}})$ . As the Coulomb interaction is spherically isotropic, a spherically-averaged model of the xc hole is often used when constructing approximate xc functionals.<sup>54</sup>

The spherically-averaged xc holes are the most negative at the position of the reference electron, and approach zero at large distance. One particular feature of the xc hole that is clearly visible in the plots in Fig. 1d is the depth of the xc hole  $\rho_{\text{xc}}^{\text{hole}}(\mathbf{r}_{\text{ref}}|\mathbf{r}_{\text{ref}}) =$

$\frac{1}{4\pi}\rho_{xc, \text{sph-av}}^{\text{hole}}(r = 0|\mathbf{r}_{\text{ref}})$ . For the  $\text{H}_2$  molecule at its equilibrium distance, the depth of the xc hole is smaller than the negative electron density, i.e., the probability of finding a second electron at the position of the reference electron is not zero. When increasing the bond distance, the depth of the xc hole increases, and in the dissociation limit it becomes equal to the negative electron density, i.e., the probability of finding a second electron at the position of the reference electron approaches zero.

## 4 Spin-State Dependent XC Holes in Two-Electron Systems: $\text{H}_2$ and He

As a first test case for exploring the spin-state dependence of the xc hole we consider two-electron systems. First, we compare the ground-state singlet state of the  $\text{H}_2$  molecule (see Section 3) to the lowest-energy triplet state. Second, we compare the singlet ground-state of the He atom ( $1s^2$ ) to its lowest energy triplet state ( $1s^12s^2$ ). Note that the total electron densities of these singlet and triplet states are in general different, which will also contribute to changes in the xc hole.

Fig. 2 shows different visualizations of the xc holes in the singlet and triplet states of the  $\text{H}_2$  molecule and the He atom. For the  $\text{H}_2$  molecule, both the equilibrium bond distance of  $d = 1.4$  bohr and the case of a dissociated  $\text{H}_2$  molecule with  $d = 5.0$  bohr are considered. In the latter case, the singlet and triplet states become degenerate and their total electron densities are equal. The reference electron is placed 0.3 bohr to the right of the right hydrogen nucleus or of the helium nucleus, respectively.

Fig. 2a compares the cylindrically-averaged xc holes of the singlet (top) and triplet (bottom) states. For the  $\text{H}_2$  molecule at  $d = 1.4$  bohr (left), the xc hole of the triplet state is more localized at the nucleus close to the reference electron than for the singlet state. In

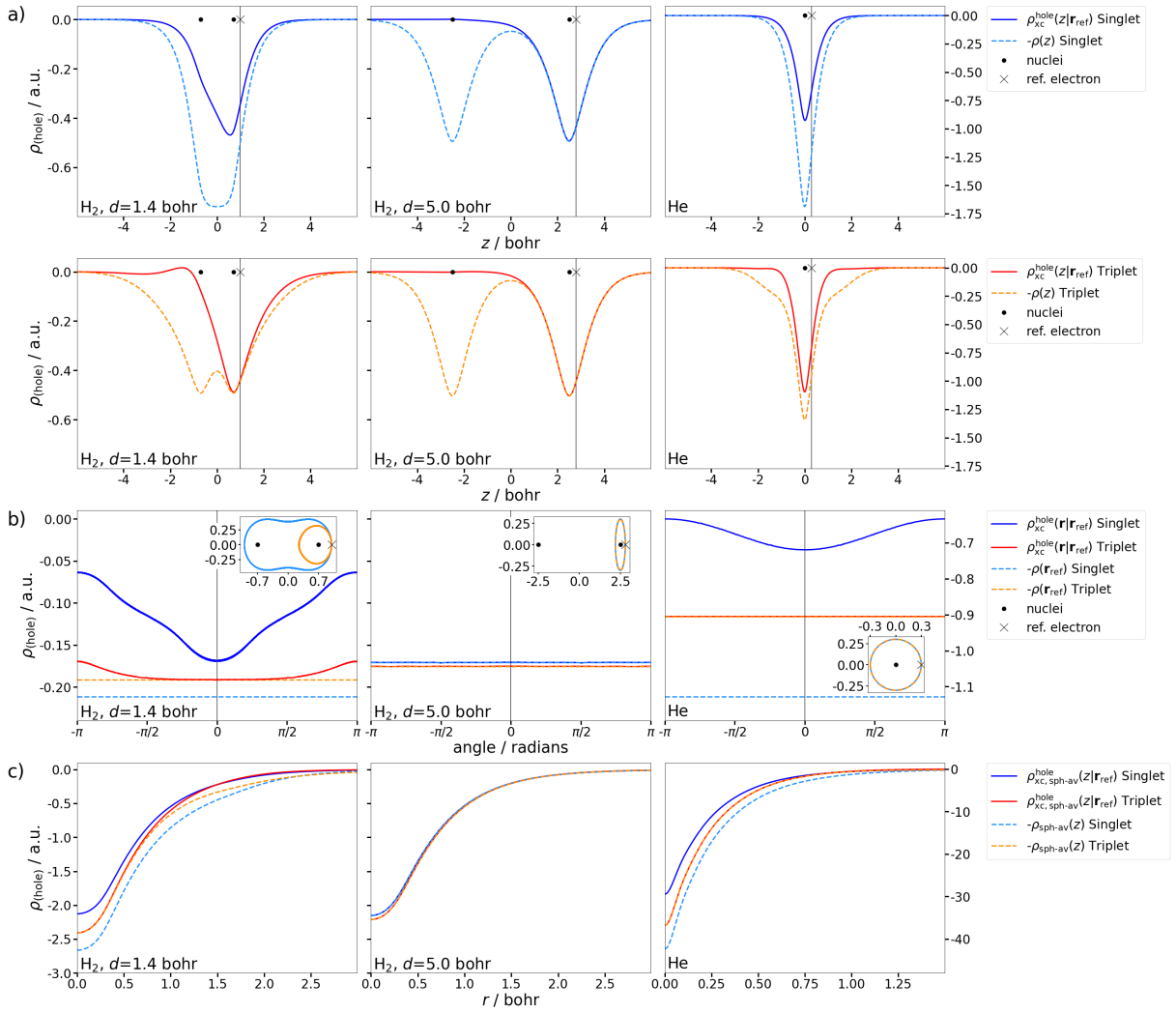


Figure 2: Comparison of the xc holes  $\rho_{\text{xc}}^{\text{hole}}(\mathbf{r}|\mathbf{r}_{\text{ref}})$  (solid lines) in the lowest-energy singlet (blue) and triplet states (red) of the H<sub>2</sub> molecule with an intermolecular distance  $d$  of 1.4 bohr (left) and 5.0 bohr (middle) and of the He atom (right). The negative electron density  $-\rho(\mathbf{r})$  (dashed light blue and orange lines for singlet and triplet states, respectively) is included for comparison. All data has been obtained from Full-CI calculations using the cc-pVTZ basis set, and the reference electron has been placed on the internuclear  $z$ -axis at a distance of 0.3 bohr from the right hydrogen atom (indicated by a cross in the plots). (a) Plots of the cylindrically-averaged negative density  $-\rho_{\text{cy-av}}(z)$  and xc hole  $\rho_{\text{xc}}^{\text{hole}}(z|\mathbf{r}_{\text{ref}})$  [cf. Eq. (35)]. (b) Plot of  $\rho_{\text{xc}}^{\text{hole}}(\mathbf{r}|\mathbf{r}_{\text{ref}})$  on a contour of constant electron density through the position of the reference electron (see inset for a visualization of these isodensity contours in the  $xz$ -plane). (c) Plot of the spherically-averaged negative density  $-\rho_{\text{sph-av}}(r)$  and xc hole  $\rho_{\text{xc}}^{\text{hole}}(r|\mathbf{r}_{\text{ref}})$  [cf. Eq. (36)].

fact, in the region of this nucleus the xc hole almost equals the negative electron density, i.e., the probability of finding a second electron at this nucleus approaches zero. While for the singlet state, the exchange hole is equal to half the negative electron density, for the triplet state it becomes localized at the nucleus close to the reference electron. On the other hand, the contribution of the correlation hole becomes significantly smaller than for the singlet state, and in the triplet state the correlation hole only leads to a small decrease of finding the second electron close to the reference electron and a corresponding increase in regions further away from the reference electron. The latter is visible in Fig. 2a as a small positive part of the xc hole between ca.  $z = -1.0$  and  $z = -2.0$  bohr and as a small difference between the negative electron density and the xc hole between ca.  $z = 2$  and  $z = 4$  bohr.

For the dissociated  $\text{H}_2$  molecule ( $d = 5.0$  bohr, middle), the xc holes of the singlet and triplet state are identical, and the xc holes are fully localized at the nucleus close to the reference electron, where it equals the negative electron density. Note that while for the singlet state, this total xc hole originates from the combination of a delocalized exchange and a delocalized correlation hole,<sup>52</sup> for the triplet state it is solely due to the exchange hole, while the correlation hole is zero in the triplet state of the dissociated  $\text{H}_2$  molecule.

For the He atom (right), the xc hole of the closed-shell singlet state is dominated by the exchange hole (i.e., half the negative electron density) and the contributions of the correlation hole are not visible in the plots of the cylindrically-averaged xc hole in Fig. 2a. For the triplet state, the electron density significantly differs from the one of the singlet state. While in a one-electron picture, the  $1s$  orbital is doubly occupied in the singlet state, the  $1s$  and  $2s$  electrons are both singly occupied in the triplet state. At the position of the reference electron, the  $1s$  orbital dominates. Therefore, the xc hole roughly corresponds to the negative of the  $1s$  orbital, i.e., given a  $1s$  electron is found at the reference position, the second electron must be in the  $2s$  orbital.

For a two-electron system, the short-range behavior of the xc hole can be analyzed by considering analytical properties of the wavefunction and the electron pair density. For a two-electron system, the wavefunction  $\Psi(\mathbf{x}_1, \mathbf{x}_2)$  can be factorized into a spatial and a spin part as,

$$\Psi(\mathbf{x}_1, \mathbf{x}_2) = \Psi(\mathbf{r}_1, \mathbf{r}_2)\sigma(s_1, s_2). \quad (37)$$

For a singlet state, the spin part is antisymmetric and the spatial part is symmetric with respect to the exchange of the two electron, while for the triplet state the spin part is symmetric and the spatial part is antisymmetric, i.e.,

$$\Psi^{S=0}(\mathbf{r}_1, \mathbf{r}_2) = +\Psi^{S=0}(\mathbf{r}_2, \mathbf{r}_1) \quad (38)$$

$$\Psi^{S=1}(\mathbf{r}_1, \mathbf{r}_2) = -\Psi^{S=1}(\mathbf{r}_2, \mathbf{r}_1). \quad (39)$$

For the singlet state, the exact short-range behavior of the wavefunction for  $\mathbf{r}_2 \rightarrow \mathbf{r}_1$  is dictated by Kato's cusp condition<sup>65-67</sup> (singlet coalescence condition),

$$\Psi^{S=0}(\mathbf{r}_1, \mathbf{r}_1 + \Delta\mathbf{r}) = \Psi^{S=0}(\mathbf{r}_1, \mathbf{r}_1) + \frac{1}{2}\Psi^{S=0}(\mathbf{r}_1, \mathbf{r}_1) |\Delta\mathbf{r}| + \mathcal{O}(|\Delta\mathbf{r}|^2). \quad (40)$$

For the triplet state, the antisymmetry of the spatial wavefunction implies that  $\Psi^{S=1}(\mathbf{r}_1, \mathbf{r}_1) = 0$ , and the cusp at the two-electron coalescence point thus vanishes while the first derivative becomes discontinuous<sup>65,67</sup> (triplet coalescence condition),

$$\Psi^{S=1}(\mathbf{r}_1, \mathbf{r}_1 + \Delta\mathbf{r}) = \Delta\mathbf{r} \cdot \left. \frac{\partial \Psi^{S=1}(\mathbf{r}_1, \mathbf{r}_1 + \Delta\mathbf{r})}{\partial |\Delta\mathbf{r}|} \right|_{|\Delta\mathbf{r}|=0} \left( 1 + \frac{1}{4}|\Delta\mathbf{r}| \right) + \mathcal{O}(|\Delta\mathbf{r}|^3). \quad (41)$$

For the electron pair density, these conditions translate to (see also Ref. 61),

$$\rho_2^{S=0}(\mathbf{r}_1, \mathbf{r}_1 + \Delta\mathbf{r}) = \rho_2^{S=0}(\mathbf{r}_1, \mathbf{r}_1) + \frac{1}{2}\rho_2^{S=0}(\mathbf{r}_1, \mathbf{r}_1) |\Delta\mathbf{r}| + \mathcal{O}(|\Delta\mathbf{r}|^2) \quad (42)$$

and

$$\rho_2^{S=1}(\mathbf{r}_1, \mathbf{r}_1 + \Delta\mathbf{r}) = \mathcal{O}(|\Delta\mathbf{r}|^2). \quad (43)$$

This different short-range behavior of the electron pair density of the singlet and triplet state can be recognized in the plots of the xc hole along the isodensity contour through the position of the reference electron that are shown in Fig. 2b. For the H<sub>2</sub> molecule at  $d = 1.4$  bohr, the xc hole of the singlet state features a cusp at the position of the reference electron when plotted along an isodensity contour, which is recovered only approximately in our finite-basis set calculations. In contrast, for the triplet state the xc hole is constant in the vicinity of the reference electron and only increases quadratically at larger distances from the reference electron. In addition, the fact that the on-top pair density  $\rho_2(\mathbf{r}, \mathbf{r})$  is zero for the triplet state is reflected by the observation that the depth of the xc hole equals the negative electron density at the position of the reference electron, while for the singlet state the on-top pair density can be nonzero and the xc hole is thus less deep.

For the H<sub>2</sub> molecule at  $d = 5.0$  bohr, the on-top pair density  $\rho_2(\mathbf{r}, \mathbf{r})$  becomes zero for both the singlet and the triplet state. Therefore, in both cases the xc hole is constant and equal to the negative electron density along an isodensity contour line through the reference electron. For the He atom, a cusp (which is recovered only approximately here) is found for the singlet state, while the xc hole is constant and equal to the negative electron density for the triplet state (see also Refs. 65,68 for an in-depth analysis of the dependence of the wavefunction of the He atom on the interelectronic distance from the perspective of wave-function theory).

Finally, the spherically averaged xc holes of the singlet and triplet states are plotted in Fig. 2c. For the H<sub>2</sub> molecule at its equilibrium bond distance and for the He atom, the differences in the on-top pair density of the singlet and triplet state discussed above are reflected by the depth of the spherically averaged xc holes at  $r = 0$ . Apart from these differences close to the position of the reference electron, the overall shape of the spherically averaged xc holes is rather similar for the singlet and triplet states. Again, for the dissociated H<sub>2</sub> molecule ( $d = 5.0$  bohr), the xc holes of the singlet and triplet state

coincide.

## 5 Spin-State Dependent XC Holes in Many-Electron Systems: $\text{Li}_2$

As a test case for a simple many-electron system, we consider the Li dimer with six electrons. In an one-electron picture of the singlet ground state of  $\text{Li}_2$ , the two 1s core orbitals of both lithium atoms are doubly occupied while the two singly occupied 2s orbitals form a  $\sigma$  bond. In the lowest energy triplet state of  $\text{Li}_2$ , these two triplet-coupled valence electrons occupy the  $\sigma$  and  $\sigma^*$  orbitals, or — in an alternative view — each sit in a 2s orbital at one of the atoms. Fig. 3 shows the xc holes for the lowest-energy singlet and triplet states of the Li dimer at its equilibrium bonds distance of 5.1 bohr as obtained from CISD calculations. We consider three different positions of the reference electron on the intermolecular  $z$ -axis at 0.3 bohr, 1.3 bohr, and 2.0 bohr to the right of the right lithium atom.

Fig. 3a plots the cylindrically-averaged xc holes of the singlet (top) and triplet (bottom) state of  $\text{Li}_2$ . For the triplet state, the cylindrically-averaged spin density of the multiplet state with  $M_S = S$ , which indicates the localization of the triplet-coupled 2s electrons, is also included. When placing the reference electron 0.3 bohr from nucleus (left), the electron density at this reference point is almost exclusively due to 1s electrons. In this case, the xc hole is very similar for the singlet and triplet state and the xc hole roughly equals half of the negative 1s electron density. Thus, no obvious difference between the spin states is observed for such a placement of the reference electron.

At the position of the reference electron 1.3 bohr from the Li nucleus (middle) both 1s and 2s electron density are present. For the singlet state, the xc hole remains localized

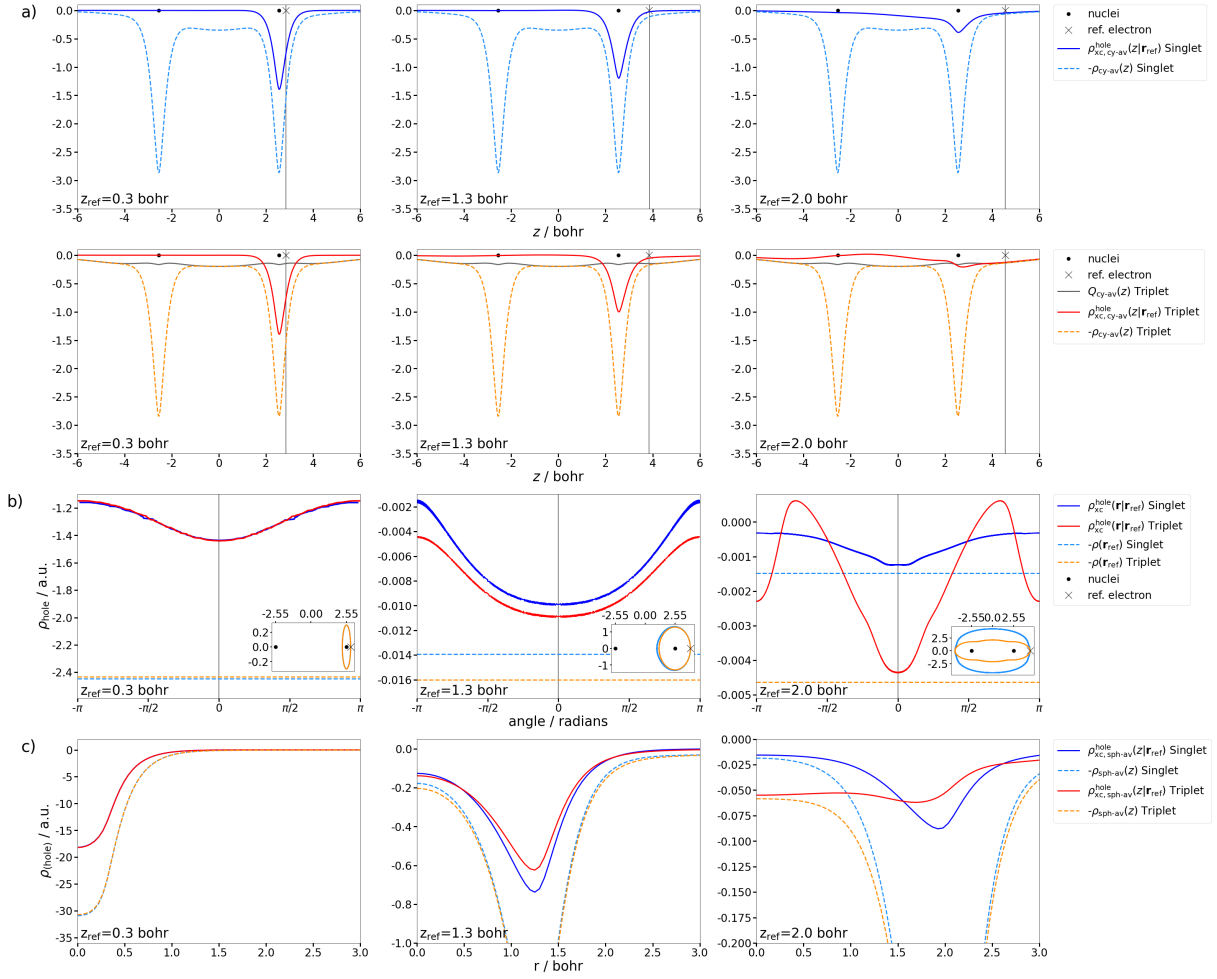


Figure 3: Comparison of the xc holes  $\rho_{\text{xc}}^{\text{hole}}(\mathbf{r}|\mathbf{r}_{\text{ref}})$  (solid lines) in the lowest-energy singlet (blue) and triplet states (red) of the Li dimer with an intermolecular distance of  $d = 5.1$  bohr. The reference electron has been placed on the internuclear  $z$ -axis at a distance of 0.3 bohr (left), 1.3 bohr (middle), and 2.0 bohr (right) from the right lithium atom (indicated by a cross in the plots). The negative electron density  $-\rho(\mathbf{r})$  (dashed light blue and orange lines for singlet and triplet states, respectively) is included for comparison. All data has been obtained from CISD calculations using the cc-pCVTZ basis set. (a) Plots of the cylindrically-averaged negative density  $-\rho_{\text{cy-av}}(z)$  and xc hole  $\rho_{\text{xc,cy-av}}^{\text{hole}}(z|\mathbf{r}_{\text{ref}})$  [cf. Eq. (35)]. For the triplet state, the cylindrically-averaged negative spin density  $-Q_{\text{cy-av}}(z)$  of the multiplet state with  $M_S = S$  is also included (black solid line). (b) Plot of  $\rho_{\text{xc}}^{\text{hole}}(\mathbf{r}|\mathbf{r}_{\text{ref}})$  on a contour of constant electron density through the position of the reference electron (see inset for a visualization of these isodensity contours in the  $xz$ -plane). (c) Plot of the spherically-averaged negative density  $-\rho_{\text{sph-av}}(r)$  and xc hole  $\rho_{\text{xc,sph-av}}^{\text{hole}}(r|\mathbf{r}_{\text{ref}})$  [cf. Eq. (36)].

at the nucleus close to reference electron, but now cancels parts of both the  $1s$  and  $2s$  electron density. For the triplet state, finding a triplet-coupled  $2s$  electron at the reference position implies that the second electron cannot occupy the same  $2s$  orbital. Therefore, xc hole of the triplet state becomes broader compared to the singlet state as it has a larger contribution resembling the  $2s$  electron density at the nucleus close to the reference electron.

The differences between the singlet and triplet states are further amplified when the reference electron is moved to 2.0 bohr from the Li nucleus (right), where the electron density is almost exclusively due to the  $2s$  electron density. For the singlet state, the xc hole remains localized at the nucleus close to the reference electron and corresponds to approximately half of the negative  $2s$  electron density at this nucleus. For the triplet state, the xc hole now fully cancels the  $2s$  electron density at the nucleus close to the reference electron and thus becomes more delocalized compared to the singlet state.

To further analyze the xc holes in the singlet and triplet state of the Li dimer, we revisit exact properties of the wavefunction and of the electron pair density in different spin states. For a many-electron system with more than two electrons, a factorization of the wavefunction into a spatial and a spin dependent part, as given in Eq. (37) for the two-electron case, is not possible,<sup>69,70</sup> i.e.,

$$\Psi(\mathbf{x}_1, \dots, \mathbf{x}_N) \neq \Psi(\mathbf{r}_1, \dots, \mathbf{r}_N)\sigma(s_1, \dots, s_N) \quad \text{for } N > 2, \quad (44)$$

and the structure of the many-electron wavefunction with respect to the exchange of spatial coordinates is intricately coupled to the spin state of the system.<sup>71</sup>

Instead, we can consider the component of the 2-RDM that determines the electron pair density,  $A(\mathbf{r}_1, \mathbf{r}_2, \mathbf{r}'_1, \mathbf{r}'_2)$ , which can be decomposed into a part that is symmetric and a part that is antisymmetric with respect to the exchange of  $\mathbf{r}_1 \leftrightarrow \mathbf{r}_2$ ,

$$A(\mathbf{r}_1, \mathbf{r}_2, \mathbf{r}'_1, \mathbf{r}'_2) = A_{\text{symm}}(\mathbf{r}_1, \mathbf{r}_2, \mathbf{r}'_1, \mathbf{r}'_2) + A_{\text{anti}}(\mathbf{r}_1, \mathbf{r}_2, \mathbf{r}'_1, \mathbf{r}'_2). \quad (45)$$

Here, the symmetric part is defined as

$$A_{\text{symm}}(\mathbf{r}_1, \mathbf{r}_2, \mathbf{r}'_1, \mathbf{r}'_2) = \frac{1}{2} \left( A(\mathbf{r}_1, \mathbf{r}_2, \mathbf{r}'_1, \mathbf{r}'_2) + A(\mathbf{r}_2, \mathbf{r}_1, \mathbf{r}'_1, \mathbf{r}'_2) \right) \quad (46)$$

with

$$A_{\text{symm}}(\mathbf{r}_1, \mathbf{r}_2, \mathbf{r}'_1, \mathbf{r}'_2) = A_{\text{symm}}(\mathbf{r}_2, \mathbf{r}_1, \mathbf{r}'_1, \mathbf{r}'_2), \quad (47)$$

and the antisymmetric part is defined as

$$A_{\text{anti}}(\mathbf{r}_1, \mathbf{r}_2, \mathbf{r}'_1, \mathbf{r}'_2) = \frac{1}{2} \left( A(\mathbf{r}_1, \mathbf{r}_2, \mathbf{r}'_1, \mathbf{r}'_2) - A(\mathbf{r}_2, \mathbf{r}_1, \mathbf{r}'_1, \mathbf{r}'_2) \right) \quad (48)$$

with

$$A_{\text{anti}}(\mathbf{r}_1, \mathbf{r}_2, \mathbf{r}'_1, \mathbf{r}'_2) = -A_{\text{anti}}(\mathbf{r}_2, \mathbf{r}_1, \mathbf{r}'_1, \mathbf{r}'_2). \quad (49)$$

In analogy to the derivation outlined in the previous section for the two-electron case, we find that the symmetric and the antisymmetric part must obey different cusp conditions analogous to the singlet coalescence condition (for the symmetric part) and the triplet coalescence condition (for the antisymmetric part). Using the above decomposition of  $A(\mathbf{r}_1, \mathbf{r}_2, \mathbf{r}'_1, \mathbf{r}'_2)$ , the electron pair density can also be decomposed into a symmetric and an antisymmetric component (see also Ref. 72, 73),

$$\rho_2(\mathbf{r}_1, \mathbf{r}_2) = \rho_2^{\text{symm}}(\mathbf{r}_1, \mathbf{r}_2) + \rho_2^{\text{anti}}(\mathbf{r}_1, \mathbf{r}_2), \quad (50)$$

with

$$\rho_2^{\text{symm}}(\mathbf{r}_1, \mathbf{r}_2) = A_{\text{symm}}(\mathbf{r}_1, \mathbf{r}_2, \mathbf{r}_1, \mathbf{r}_2) \quad (51)$$

$$\rho_2^{\text{anti}}(\mathbf{r}_1, \mathbf{r}_2) = A_{\text{anti}}(\mathbf{r}_1, \mathbf{r}_2, \mathbf{r}_1, \mathbf{r}_2). \quad (52)$$

These symmetric and antisymmetric components of the electron pair density exhibit a different exact short-range behavior, which is given by

$$\rho_2^{\text{symm}}(\mathbf{r}_1, \mathbf{r}_1 + \Delta\mathbf{r}) = \rho_2^{\text{symm}}(\mathbf{r}_1, \mathbf{r}_1) + \frac{1}{2} \rho_2^{\text{symm}}(\mathbf{r}_1, \mathbf{r}_1) |\Delta\mathbf{r}| + \mathcal{O}(|\Delta\mathbf{r}|^2) \quad (53)$$

and

$$\rho_2^{\text{anti}}(\mathbf{r}_1, \mathbf{r}_1 + \Delta\mathbf{r}) = \mathcal{O}(|\Delta\mathbf{r}|^2). \quad (54)$$

The relative contribution of the symmetric and antisymmetric components to the electron spin density depends on the spin state of the system. This is most obvious for the two-electron systems considered in the previous section, where the antisymmetric part vanishes for singlet states, whereas the symmetric part vanishes for triplet states. In Appendix A, we demonstrate that the normalization of the symmetric and antisymmetric parts of the electron pair density is determined by the spin state.

For the Li dimer as a four electron system, the total electron pair density is normalized to  $N(N - 1) = 12$ . Using the result of Appendix A, we find that for the singlet state,

$$\iint \rho_2^{\text{symm}}(\mathbf{r}_1, \mathbf{r}_2) d^3r_1 d^3r_2 = 6 \quad \text{and} \quad \iint \rho_2^{\text{anti}}(\mathbf{r}_1, \mathbf{r}_2) d^3r_1 d^3r_2 = 6 \quad (55)$$

whereas for the triplet state

$$\iint \rho_2^{\text{symm}}(\mathbf{r}_1, \mathbf{r}_2) d^3r_1 d^3r_2 = 4 \quad \text{and} \quad \iint \rho_2^{\text{anti}}(\mathbf{r}_1, \mathbf{r}_2) d^3r_1 d^3r_2 = 8. \quad (56)$$

To some extent, the different contributions of the symmetric and antisymmetric components of the electron pair density can be seen in the plots of the xc holes of the singlet and triplet states along isodensity contours through the reference electron, which are shown in Fig. 3b. If the reference electron is 0.3 bohr from the Li nucleus (left), where the electron density is solely due to singlet-coupled electrons, the relative contributions of the symmetric and antisymmetric components are equal for the singlet and triplet state and, consequently, the short-range behavior of the xc hole is identical for both states. Along the isodensity contour, the xc hole should show a cusp at the position of the reference electron which is due to the symmetric component of the electron pair density. Note, however, that in our finite-basis set calculations this cusp is only recovered approximately.

When positioning the reference electron 1.3 bohr from the Li nucleus (middle), the xc hole along the isodensity contour should still exhibit a cusp at the position of the reference electron for both the singlet and triplet state. Since for the triplet state, parts of the electron density at the reference point are due to triplet coupled electrons, the relative contribution of the antisymmetric part of the electron pair density should increase. While it is obvious that the xc holes along the isodensity contour differ, different cusp conditions are not discernible from the plots because of the insufficiencies of our finite basis set treatment. For a placement of the reference electron 2.0 from the Li nucleus (right), the xc hole of the triplet state should now be almost exclusively due to the antisymmetric part of the electron pair density. Unfortunately, the different cusp conditions are masked by the fact that on the one hand, the electron pair density at the position of the reference electron becomes very small also for the singlet state, and that on the other hand there are large changes of the xc hole of the triplet state along the isodensity contour. The latter are caused by changes in the contribution of the  $2s$  electron density along the isodensity contour. Here, further analysis of the short-range behavior using larger basis sets or explicitly correlated methods<sup>65</sup> could possibly reveal further details.

Finally, Fig. 3c plots the spherically averaged xc holes of the singlet and triplet state in  $\text{Li}_2$ . Again, if the reference electron is 0.3 bohr from the Li nucleus (left), the xc holes of the singlet and triplet state are identical. The depth of the xc hole is more than half of the electron density at the position of the reference electron, but there also remains a large probability for finding the second electron at the position of the reference electron. For a reference position 1.3 bohr from the Li nucleus (middle) the depth of the xc hole gets closer to the electron density at the position of the reference point. Overall, the spherically-averaged singlet and triplet xc holes remain rather similar. If the reference electron is placed 2.0 bohr from the Li nucleus, the depth of the xc hole becomes approximately equal to the electron density at the reference point. While this electron density differs for the singlet and triplet state, the short-range behavior of the

spherically-averaged xc holes is again very similar for both states. At larger distances from the reference electron, differences appear that mirror the different long-range parts of the xc holes that have been discussed above.

## 6 Conclusions and Perspectives

Here, we have analyzed the xc holes extracted from wavefunction-based configuration interaction calculations for the lowest-energy singlet and triplet states for simple model systems. In particular, we have considered the  $\text{H}_2$  molecule at different internuclear distances and the helium atom as prototypical two-electron systems as well as the Li dimer as a simple many-electron system. First, we find that in all cases, the total xc hole is in general localized in the vicinity of the reference electron, whereas the individual exchange and correlation holes can be rather delocalized.<sup>52</sup> Moreover, the total xc holes of the singlet and triplet states are more similar to each other than the individual exchange and correlation holes.

This is most obvious for the  $\text{H}_2$  molecule at large intermolecular separation, in which the singlet and triplet states become degenerate and feature identical total xc holes, while their decomposition into exchange and correlation holes is very different. The well-known empirical findings that spin-state energy differences can be tuned by varying the amount of exact exchange admixture<sup>19,20</sup> is a consequence of the different decomposition of the total xc hole into exchange and correlation contributions in different spin states. Our observation that the total xc holes of singlet and triplet states show more common features than the individual exchange and correlation holes reaffirms our assumption that modeling the total xc hole instead of the individual exchange and correlation holes might be a promising strategy for the development of explicitly spin-state dependent approximations to the xc functional.

The most obvious difference between the xc holes of singlet and triplet states is the different depth of the xc hole, which is directly related to the on-top pair density  $\rho_2(\mathbf{r}, \mathbf{r})$ . For two-electron systems, the depth of the xc hole equals the negative electron density at the position of the reference electron in the triplet state, while it is generally less deep for the singlet state. For many-electron systems, we have established a decomposition of the electron pair density into a symmetric component (which obeys a singlet coalescence condition) and an antisymmetric component (which obeys a triplet coalescence condition). By analyzing the spin-state dependence of the 2-RDM, we have shown that the relative contributions of these two components are directly determined by the spin state. This might provide a route to the construction of explicitly spin-state dependent approximations to the xc functional.

However, the relative contributions of the symmetric and antisymmetric components of the electron pair density are different in different regions of space, i.e., they depend on the localization of the electrons for which the spin coupling differs. Thus, the construction of explicitly spin-state dependent approximations to the xc functional will require accounting for this spatial distribution of spin coupling effects. Most likely, this will require using a suitable auxiliary quantity in addition to the total electron density.

The most straight-forward approach would be using the (exact or approximate) on-top pair density for constructing approximations of the xc hole. Such a strategy is used in the context of methods combining a multideterminantal reference system with a density functional treatment of dynamic correlation.<sup>38,74-77</sup> However, in such approaches the spin-state dependence is included via the spin-state of the multideterminantal wavefunction and not included explicitly in the xc functional.

Alternatively, one could model the (spin-state dependent) on-top pair density as a functional of the total electron density and another auxiliary quantity. Conventionally, the spin density of the state with  $M_S = S$  is used to this end, and it has been shown that

within such a picture the local spin-density approximation provides a very accurate approximation of the on-top pair density.<sup>78</sup> However, we are convinced that the use of the spin density for modeling the spin-state dependence is undesirable, as it implies a violation of the fractional spin condition.<sup>42</sup> Alternatively, the spin density could be reinterpreted as on-top pair density as suggested by Perdew et al.,<sup>79</sup> which could offer a possible route to the construction of explicitly spin-state dependent models of the xc hole. Finally, we note that Staroverov and Davidson have suggested using the singlet and triplet densities that arise from our symmetric and antisymmetric components of the electron pair density by integration over  $\mathbf{r}_2$  as fundamental quantities for the construction of approximate xc functionals.

We hope that this study sheds some light on the treatment of spin states in density-functional theory, and that it will inspire future work towards the construction of explicitly spin-state dependent exchange–correlation functionals.

## Computational Details

All configuration interaction (CI) calculations have been performed using PySCF.<sup>80,81</sup> For the two-electron systems, PySCF’s full configuration interaction module FCI has been used, whereas for the Li dimer the configuration interaction with single and double excitations module CISD was used. For the triplet states, our CI calculations started from a spin-restricted open-shell Hartree-Fock determinant to ensure that the resulting CI solution is a pure spin state. The cc-pVTZ basis<sup>82</sup> set was employed for the H<sub>2</sub> and the He atom, whereas the cc-pCVTZ basis set<sup>83</sup> was used for the Li dimer in order to capture core correlation effects.

PySCF gives access to the of the 2-RDM in the molecular orbital basis,

$$\Gamma_2(\mathbf{r}_1, \mathbf{r}_2, \mathbf{r}'_1, \mathbf{r}'_2) = \sum_{pqrs} c_{pqrs} \phi_p(\mathbf{r}_1) \phi_q(\mathbf{r}_2) \phi_r(\mathbf{r}'_1) \phi_s(\mathbf{r}'_2), \quad (57)$$

from which the xc hole can be calculated according to Eq. (29).

All plots have been prepared using Matplotlib.<sup>84,85</sup> A Jupyter notebook that can be used to obtain all the plots presented here is made available on GitHub at <https://github.com/chjacob-tubs/xcholes>.

## Acknowledgments

This paper is dedicated to Prof. Evert-Jan Baerends (VU University Amsterdam), whose pioneering work on exchange–correlation holes inspired our study, on the occasion of his upcoming 75th birthday.

## A Spin-state dependence of the normalization of

$$\rho_2^{\text{symm}}(\mathbf{r}_1, \mathbf{r}_2) \text{ and } \rho_2^{\text{anti}}(\mathbf{r}_1, \mathbf{r}_2)$$

The normalization of the electron pair density is given by

$$\begin{aligned} & \iint \rho_2(\mathbf{r}_1, \mathbf{r}_2) d^3r_1 d^3r_2 \\ &= \iint \rho_2^{\text{symm}}(\mathbf{r}_1, \mathbf{r}_2) d^3r_1 d^3r_2 + \iint \rho_2^{\text{anti}}(\mathbf{r}_1, \mathbf{r}_2) d^3r_1 d^3r_2 = N(N+1). \end{aligned} \quad (58)$$

Using the definitions of the symmetric and antisymmetric parts of  $A(\mathbf{r}_1, \mathbf{r}_2, \mathbf{r}'_1, \mathbf{r}'_2)$  [cf. Eqs. (46) and (48)], the expression for the calculation of the expectation value of the total

spin operator given in Eq. (21) can be recast as,

$$\begin{aligned}\langle \hat{\mathbf{S}}^2 \rangle &= -\frac{1}{4} \iint \left( 3A_{\text{symm}}(\mathbf{r}_1, \mathbf{r}_2, \mathbf{r}_1, \mathbf{r}_2) - A_{\text{anti}}(\mathbf{r}_1, \mathbf{r}_2, \mathbf{r}_1, \mathbf{r}_2) \right) d^3r_1 d^3r_2 + \frac{3}{4}N \\ &= -\frac{3}{4} \iint \rho_2^{\text{symm}}(\mathbf{r}_1, \mathbf{r}_2) d^3r_1 d^3r_2 + \frac{1}{4} \iint \rho_2^{\text{anti}}(\mathbf{r}_1, \mathbf{r}_2) d^3r_1 d^3r_2 + \frac{3}{4}N\end{aligned}\quad (59)$$

and it follows that

$$3 \iint \rho_2^{\text{symm}}(\mathbf{r}_1, \mathbf{r}_2) d^3r_1 d^3r_2 - \iint \rho_2^{\text{anti}}(\mathbf{r}_1, \mathbf{r}_2) d^3r_1 d^3r_2 = 3N - 4\langle \hat{\mathbf{S}}^2 \rangle \quad (60)$$

Combining Eqs. (58) and (60), we find

$$\iint \rho_2^{\text{symm}}(\mathbf{r}_1, \mathbf{r}_2) d^3r_1 d^3r_2 = \frac{1}{4}N^2 + \frac{1}{2}N - \langle \hat{\mathbf{S}}^2 \rangle \quad (61)$$

$$\iint \rho_2^{\text{anti}}(\mathbf{r}_1, \mathbf{r}_2) d^3r_1 d^3r_2 = \frac{3}{4}N^2 - \frac{3}{2}N + \langle \hat{\mathbf{S}}^2 \rangle. \quad (62)$$

Thus, when increasing  $\langle \hat{\mathbf{S}}^2 \rangle$ , the normalization of the antisymmetric part increases, while the one of the symmetric part decreases. The above result has previously been obtained for the corresponding singlet and triplet densities in a slightly different way by Davidson *et al.*<sup>72,73</sup>

## References

- [1] M. Reiher, *Chimia*, 2009, **63**, 140–145.
- [2] S. Ye and F. Neese, *Inorg. Chem.*, 2010, **49**, 772–774.
- [3] M. Radoń, *J. Chem. Theory Comput.*, 2014, **10**, 2306–2321.
- [4] M. Atanasov, D. Aravena, E. Suturina, E. Bill, D. Maganas, and F. Neese, *Coord. Chem. Rev.*, 2015, **289-290**, 177–214.
- [5] A. Ghosh, *Chem. Rev.*, 2017, **117**, 3798–3881.

- [6] A. R. Finkelmann, M. T. Stiebritz, and M. Reiher, *J. Phys. Chem. B*, 2013, **117**, 4806–4817.
- [7] V. Krewald, M. Retegan, N. Cox, J. Messinger, W. Lubitz, S. DeBeer, F. Neese, and D. A. Pantazis, *Chem. Sci.*, 2015.
- [8] K. D. Vogiatzis, M. V. Polynski, J. K. Kirkland, J. Townsend, A. Hashemi, C. Liu, and E. A. Pidko, *Chem. Rev.*, 2018.
- [9] J. Rudolph and Ch. R. Jacob, *ACS Omega*, 2019, **4**, 7987–7993.
- [10] S. Schinzel, J. Schraut, A. V. Arbuznikov, P. E. M. Siegbahn, and M. Kaupp, *Chem. Eur. J.*, 2010, **16**, 10424–10438.
- [11] A. Boubnov, H. W. P. Carvalho, D. E. Doronkin, T. Günter, E. Gallo, A. J. Atkins, Ch. R. Jacob, and J.-D. Grunwaldt, *J. Am. Chem. Soc.*, 2014, **136**, 13006–13015.
- [12] T. Günter, H. W. P. Carvalho, D. E. Doronkin, T. Sheppard, P. Glatzel, A. J. Atkins, J. Rudolph, Ch. R. Jacob, M. Casapu, and J.-D. Grunwaldt, *Chem. Commun.*, 2015, **51**, 9227–9230.
- [13] S. N. MacMillan and K. M. Lancaster, *ACS Catalysis*, 2017, **7**, 1776–1791.
- [14] J. Rudolph and Ch. R. Jacob, *Inorg. Chem.*, 2018, **57**, 10591–10607.
- [15] C. Herrmann, G. C. Solomon, and M. A. Ratner, *J. Chem. Phys.*, 2011, **134**, 224306.
- [16] C. Herrmann, *J. Phys. Chem. A*, 2019, p. acs.jpca.9b05618.
- [17] J. N. Harvey, *Struct. Bond.*, 2004, **112**, 151–184.
- [18] C. J. Cramer and D. G. Truhlar, *Phys. Chem. Chem. Phys.*, 2009, **11**, 10757.
- [19] M. Swart, *Int. J. Quantum Chem.*, 2013, **113**, 2–7.
- [20] M. Reiher, O. Salomon, and B. A. Hess, *Theor. Chem. Acc.*, 2001, **107**, 48–55.

- [21] M. Swart, *J. Chem. Theory Comput.*, 2008, **4**, 2057–2066.
- [22] M. Radoń, *Phys. Chem. Chem. Phys.*, 2014, **16**, 14479–14488.
- [23] M. Swart, M. Sola, and F. M. Bickelhaupt, *J. Chem. Phys.*, 2009, **131**, 094103.
- [24] M. Swart, *Chem. Phys. Lett.*, 2013, **580**, 166–171.
- [25] K. Pierloot, *Mol. Phys.*, 2003, **101**, 2083–2094.
- [26] K. Pierloot, Q. M. Phung, and A. Domingo, *J. Chem. Theory Comput.*, 2017, **13**, 537–553.
- [27] M. Radoń, *Phys. Chem. Chem. Phys.*, 2019, **21**, 4854–4870.
- [28] P. G. Szalay, T. Müller, G. Gidofalvi, H. Lischka, and R. Shepard, *Chem. Rev.*, 2012, **112**, 108–181.
- [29] S. Ghosh, P. Verma, C. J. Cramer, L. Gagliardi, and D. G. Truhlar, *Chem. Rev.*, 2018, **118**, 7249–7292.
- [30] K. H. Marti and M. Reiher, *Phys. Chem. Chem. Phys.*, 2011, **13**, 6750–6759.
- [31] G. K.-L. Chan and S. Sharma, *Annu. Rev. Phys. Chem.*, 2011, **62**, 465–481.
- [32] A. Baiardi and M. Reiher, *J. Chem. Phys.*, 2020, **152**, 040903.
- [33] S. Sharma and G. K.-L. Chan, *J. Chem. Phys.*, 2012, **136**, 124121.
- [34] S. Wouters, P. A. Limacher, D. Van Neck, and P. W. Ayers, *J. Chem. Phys.*, 2012, **136**, 134110.
- [35] Y. Kurashige and T. Yanai, *J. Chem. Phys.*, 2011, **135**, 094104.
- [36] M. Roemelt, S. Guo, and G. K. L. Chan, *J. Chem. Phys.*, 2016, **144**, 204113.

- [37] L. Freitag, S. Knecht, C. Angeli, and M. Reiher, *J. Chem. Theory Comput.*, 2017, **13**, 451–459.
- [38] G. Li Manni, R. K. Carlson, S. Luo, D. Ma, J. Olsen, D. G. Truhlar, and L. Gagliardi, *J. Chem. Theory Comput.*, 2014.
- [39] E. D. Hedegård, S. Knecht, J. S. Kielberg, H. J. A. Jensen, and M. Reiher, *J. Chem. Phys.*, 2015, **142**, 224108.
- [40] L. Gagliardi, D. G. Truhlar, G. Li Manni, R. K. Carlson, C. E. Hoyer, and J. L. Bao, *Acc. Chem. Res.*, 2017, **50**, 66–73.
- [41] S. J. Stoneburner, D. G. Truhlar, and L. Gagliardi, *J. Chem. Phys.*, 2018, **148**, 064108.
- [42] Ch. R. Jacob and M. Reiher, *Int. J. Quantum Chem.*, 2012, **112**, 3661–3684.
- [43] P. Hohenberg and W. Kohn, *Phys. Rev.*, 1964, **136**, B864–B871.
- [44] M. Levy, *Proc. Natl. Acad. Sci. U. S. A.*, 1979, **76**, 6062–6065.
- [45] J. P. Perdew, R. G. Parr, M. Levy, and J. L. Balduz Jr., *Phys. Rev. Lett.*, 1982, **49**, 1691.
- [46] O. Gunnarsson and B. I. Lundqvist, *Phys. Rev. B*, 1976, **13**, 4274–4298.
- [47] A. J. Cohen, P. Mori-Sanchez, and W. Yang, *J. Chem. Phys.*, 2008, **129**, 121104.
- [48] A. J. Cohen, P. Mori-Sanchez, and W. Yang, *Science*, 2008, **321**, 792–794.
- [49] A. J. Cohen, P. Mori-Sánchez, and W. Yang, *Chem. Rev.*, 2012, **112**, 289–320.
- [50] R. McWeeny and B. T. Sutcliffe, *Methods of Molecular Quantum Mechanics*, Academic Press, New York, 1969.

- [51] R. G. Parr and W. Yang, *Density-Functional Theory of Atoms and Molecules*, Oxford University Press, Oxford, 1989.
- [52] E. J. Baerends and O. V. Gritsenko, *J. Phys. Chem. A*, 1997, **101**, 5383–5403.
- [53] M. A. Buijse and E. J. Baerends in *Density Functional Theory of Molecules, Clusters, and Solids*, ed. D. E. Ellis; Kluwer, Dordrecht, 1994.
- [54] M. Ernzerhof, J. P. Perdew, and K. Burke in *Density Functional Theory I*, ed. P. R. F. Nalewajski, Topics in Current Chemistry; Springer Berlin Heidelberg, 1996; pp. 1–30.
- [55] A. D. Becke and M. R. Roussel, *Phys. Rev. A*, 1989, **39**, 3761–3767.
- [56] A. D. Becke, *J. Chem. Phys.*, 2003, **119**, 2972–2977.
- [57] A. D. Becke, *J. Chem. Phys.*, 2013, **138**, 074109.
- [58] H. Bahmann and M. Ernzerhof, *J. Chem. Phys.*, 2008, **128**, 234104.
- [59] J. Přecechtělová, H. Bahmann, M. Kaupp, and M. Ernzerhof, *J. Chem. Phys.*, 2014, **141**, 111102.
- [60] R. McWeeny and Y. Mizuno, *Proc. Roy. Soc. Ser. A*, 1961, **259**, 554–577.
- [61] E. R. Davidson, *Reduced Density Matrices in Quantum Chemistry*, Academic Press, New York, 1976.
- [62] M. J. G. Peach, A. M. Teale, and D. J. Tozer, *J. Chem. Phys.*, 2007, **126**, 244104.
- [63] M. J. G. Peach, A. M. Miller, A. M. Teale, and D. J. Tozer, *J. Chem. Phys.*, 2008, **129**, 064105.
- [64] A. M. Teale, S. Coriani, and T. Helgaker, *J. Chem. Phys.*, 2010, **132**, 164115.
- [65] C. Hättig, W. Klopper, A. Köhn, and D. P. Tew, *Chem. Rev.*, 2012, **112**, 4–74.

- [66] T. Kato, *Communications on Pure and Applied Mathematics*, 1957, **10**, 151–177.
- [67] R. T. Pack and W. B. Brown, *J. Chem. Phys.*, 1966, **45**, 556–559.
- [68] D. P. Tew, W. Klopper, and T. Helgaker, *J. Comput. Chem.*, 2007, **28**, 1307–1320.
- [69] F. A. Matsen, *Adv. Quantum Chem.*, 1964, **1**, 59–114.
- [70] R. Pauncz, *Spin Eigenfunctions*, Plenum Press, New York, 1979.
- [71] R. Pauncz, *The Symmetric Group in Quantum Chemistry*, CRC-Press, Boca Raton, FL, 1995.
- [72] E. R. Davidson, *Int. J. Quantum Chem.*, 1998, **69**, 241–245.
- [73] V. N. Staroverov and E. R. Davidson, *Int. J. Quantum Chem.*, 2000, **77**, 651–660.
- [74] A. D. Becke, A. Savin, and H. Stoll, *Theor. Chim. Acta*, 1995, **91**, 147–156.
- [75] S. Gusarov, P.-Å. Malmqvist \*, and R. Lindh, *Mol. Phys.*, 2004, **102**, 2207–2216.
- [76] A. Ferté, E. Giner, and J. Toulouse, *J. Chem. Phys.*, 2019, **150**, 084103.
- [77] M. Hapka, E. Pastorczak, A. Krzemińska, and K. Pernal, *J. Chem. Phys.*, 2020, **152**, 094102.
- [78] K. Burke, J. P. Perdew, and M. Ernzerhof, *J. Chem. Phys.*, 1998, **109**, 3760–3771.
- [79] J. P. Perdew, M. Ernzerhof, K. Burke, and A. Savin, *Int. J. Quantum Chem.*, 1997, **61**, 197–205.
- [80] Q. Sun, T. C. Berkelbach, N. S. Blunt, G. H. Booth, S. Guo, Z. Li, J. Liu, J. D. McClain, E. R. Sayfutyarova, S. Sharma, S. Wouters, and G. K.-L. Chan, *WIREs Comput. Mol. Sci.*, 2018, **8**, e1340.
- [81] PySCF Version 1.7.1, DOI: 10.5281/zenodo.3692842, URL: <https://sunqm.github.io>, 2020.

- [82] J. Dunning, *J. Chem. Phys.*, 1989, **90**, 1007–1023.
- [83] D. E. Woon and T. H. Dunning Jr, *J. Chem. Phys.*, 1998, **103**, 4572.
- [84] J. D. Hunter, *Comput. Sci. Eng.*, 2007, **9**, 90–95.
- [85] MATPLOTLIB Version 3.2.1, DOI: 10.5281/zenodo.3714460, URL:  
<https://matplotlib.org>, 2020.